JM PAPERS

Asymptotic matching modal model on Richtmyer–Meshkov instability

Jiaxuan Li[1], Chenren Chen[1], Zhigang Zhai[1,2],† and Xisheng Luo[1,2],†

[1]Advanced Propulsion Laboratory, Department of Modern Mechanics, University of Science and Technology of China, Hefei 230026, PR China

[2]State Key Laboratory of High Temperature Gas Dynamics, Institute of Mechanics, Chinese Academy of Sciences, Beijing 100190, PR China

An asymptotic matching modal model is established based on the singular perturbation method for predicting mode evolution in single- and dual-mode interfaces accelerated by a shock wave. The startup process is incorporated into the model to provide a complete description of the mode evolution after the shock impact. Through considering the feedback from high-order harmonic to the third-order harmonic, the model accuracy is improved and the model divergence is prevented. In addition, the model can evaluate the mutual-coupling effect on the amplitude variations of high-order harmonics besides the 'beat modes'. To validate the model, experiments on both light–heavy and heavy–light interfaces subject to a shock wave are conducted, and both single- and dual-mode interfaces formed by the soap-film technique are involved. The interface profiles extracted from mode decomposition and predicted by the model show high consistency with the experimental counterparts. Good agreement of the mode amplitude growths between the experiments and theoretical predictions shows the superiority of the model, especially for the heavy–light interface.

1. Introduction

Richtmyer–Meshkov instability (RMI) arises when a perturbed interface separating fluids with disparate physical properties is accelerated by a shock wave (Richtmyer 1960; Meshkov 1969). It is generally considered as an impulsive version of Rayleigh–Taylor instability (RTI), which occurs only when a heavy fluid is accelerated by a light fluid (Rayleigh 1882; Taylor 1950); RMI is an important phenomenon occurring in many applications (Prestridge 2018; Zhou *et al.* 2019). For example, in inertial confinement

† Email addresses for correspondence: sanjing@ustc.edu.cn, xluo@ustc.edu.cn

fusion reactions, the mixing induced by RMI results in fuel contamination and limits the fusion energy gain (Chu *et al.* 2022; Hurricane *et al.* 2023). It is therefore essential to comprehend the evolution of RMI on the target interface (Zhou 2017; Zhai *et al.* 2018; Liang & Luo 2023).

The RMI of a single-mode interface has been widely investigated theoretically. In the linear stage, the interface profile is dominated by the fundamental mode, which exists on the initial interface. As the interface evolves into nonlinear stages, higher-order harmonics with wavenumbers being integer multiples of the fundamental mode wavenumber are generated and grow. This process is referred to as the self-coupling of the fundamental mode. Richtmyer (1960) first derived the linearized governing equation for the single-mode RMI growth. Subsequently, various models for linear growth (Meyer & Blewett 1972; Yang, Zhang & Sharp 1994; Wouchuk & Nishihara 1997; Wouchuk 2001) and nonlinear growth (Dimonte & Ramaprabhu 2010; Zhang & Guo 2016) have been established through diverse physical hypotheses. Recently, a unified theoretical model for spatiotemporal development of Richtmyer–Meshkov fingers was proposed by combining the classical potential flow theory with a dual-source model (Liu, Zhang & Xiao 2023). In addition, by incorporating different physical mechanisms into the analytical models, the three-dimensional (3-D) effect (Chapman & Jacobs 2006; Luo *et al.* 2016), the geometric effect (Luo *et al.* 2019; Ge *et al.* 2022), the high-amplitude effect (Wang *et al.* 2023*b*; Dimonte *et al.* 2024), the Atwood number (defined as $A = (\rho_2 - \rho_1)/(\rho_2 + \rho_1)$, with ρ_2 and ρ_1 being the fluid densities at each side of the interface) effect (Chen *et al.* 2019, 2023), the interface coupling effect (Liang & Luo 2023; Schalles 2023) and the Mach number effect (Motl *et al.* 2009) have been evaluated.

In practical situations, random multi-mode perturbations are commonly present on initial interfaces, which means that more than one fundamental mode exists on the initial interface. Therefore, besides self-coupling of each individual fundamental mode, the different fundamental modes will also couple together in the multi-mode RMI, which is referred to as the mutual coupling between two fundamental modes. To characterize the perturbation growth of the multi-mode RMI, several theoretical approaches were adapted and improved from single-mode situations (Vandenboomgaerde, Gauthier & Mügler 2002). A single bubble potential model was developed by Layzer (1955), and various models have been derived since then through the potential flow method with different potential functions and mathematical treatments. Starting from the potential flow method, the perturbation expansion technique was employed to model the modal evolution of the single-mode RMI by considering the interface perturbation as a superposition of various Fourier modes (Zhang & Sohn 1997). Besides, Haan (1991) proposed a second-order solution for multi-mode classical RTI growth (the Haan model). The Haan model and its variations have been verified extensively through simulations and high energy density experiments (Remington *et al.* 1995; Ofer *et al.* 1996; Di Stefano *et al.* 2017; Elbaz & Shvarts 2018).

In the models mentioned above, the linear growth of the amplitude was satisfied after the shock impact, while the starting point of theoretical prediction was chosen artificially. Note that an implicit initial condition for shock–interface interaction is that the perturbation growth rate is zero, not a finite value, immediately after the shock impact (Fraley 1986; Yang *et al.* 1994). This means that the amplitude growth rate will experience an acceleration from zero to an asymptotic value after the shock impact, which is referred to as the startup process. In some linear compressible analytical models (Richtmyer 1960; Yang *et al.* 1994; Wouchuk & Nishihara 1997; Wouchuk 2001; Cobos Campos & Wouchuk 2014, 2016), the authors have already discussed the startup process,

and have identified two main contributions to the asymptotic growth rate: the vorticity deposited at the interface by shock refraction, and the acoustic interaction of the perturbed interface with the shock front. This interaction is responsible for the oscillatory evolution of the growth rate. However, in some linear compressible analytical models (Richtmyer 1960; Yang *et al.* 1994), the startup process was solved numerically, and there are no analytical solutions. Although there are infinite series solutions to the startup process in the linear model proposed by Wouchuk & Nishihara (1997), the form of the solutions is complicated. In addition, the startup process is rarely considered in previous nonlinear analytical models, many of which were derived based on the initial conditions of linear growth. Vandenboomgaerde *et al.* (2002) matched their nonlinear theory to the early-time compressible phase without considering the startup process, which may lead to an obvious shift between theoretical predictions and numerical data, as given in figure 2(*a*) in their work. As a result, the nonlinear evolution of the perturbation immediately after the shock impact cannot be fully described by the existing nonlinear models due to the ignorance of the startup process.

Recently, Zhang, Deng & Guo (2018) proposed a quantitative theory for the single-mode RMI that covers the entire time domain from early to late times based on the two-point Padé approximation method. This is the first nonlinear model that considers the startup process, to our best knowledge. However, it should be noted that the matching technique employed by Zhang *et al.* (2018) introduces the nonlinear trend from the beginning of the interface evolution, not after the startup process, which may be inappropriate for the potential flow method. The startup process was investigated in detail, respectively, for a light–heavy interface (Lombardini & Pullin 2009) and a heavy–light interface (Li *et al.* 2024), and it was concluded that the startup time is in proportion to the perturbation wavelength. Therefore, for an initially multi-mode interface, the fundamental modes have diverse startup times since the wavelengths for the fundamental modes are different. In particular, for a heavy–light interface, there is a unique phenomenon, called phase inversion, that may occur during or after the startup process (Li *et al.* 2024). The prediction of the phase inversion has never been achieved in previous modal models. Considering the presence of complex processes such as phase inversion in the early evolution of RMI, the startup process must be considered in the model. Also, the lower accuracy of the modal model will cause divergence for predicting the amplitude growths of the high-order harmonics. Considering the startup process will not only make the model more approximate to the physical assumptions of initial conditions of linear growth, but also improve the accuracy of the theoretical predictions. Nevertheless, it is challenging to establish a model that can characterize the diverse startup times of different fundamental modes to give a complete mode evolution after the shock impact, and demonstrate the mode-coupling effects on different harmonics. These concerns motivate the current work.

In this study, an asymptotic matching modal model is established for RMI. The startup process is incorporated into the model to provide a complete description of the mode evolution after the shock impact. Through considering the feedback from high-order harmonic to the third-order harmonic, the model accuracy is improved and the model divergence is prevented. In addition, the model can evaluate the mutual-coupling effect on the amplitude variations of high-order harmonics besides the 'beat modes'. In the following, first the derivation of the model is provided. Then experiments on single- and dual-mode interfaces subject to a shock wave are conducted to verify the model. In experiments, both the light–heavy and heavy–light interfaces are involved. The amplitudes of different modes are extracted from the experiments and compared with the predictions from the model.

2. Theoretical derivation

2.1. *Classical modal models*

Modal models are a class of potential flow models that are capable of describing the Fourier mode evolution. The amplitude of jth-order interface mode is defined as

$$a_j(t) = \lambda^{-1} \int \exp(-2\mathrm{i}j\pi x/\lambda)\, a(x, t)\, \mathrm{d}x, \tag{2.1}$$

where λ is the perturbation wavelength for one period, $k_j = 2j\pi/\lambda$ is the jth-order perturbation wavenumber, i is the imaginary unit, and $a(x, t)$ represents the interface profile. Starting from the potential flow method, the perturbation expansion technique was employed to model the modal evolution of the single-mode RMI by considering the interface perturbation as a superposition of various Fourier modes (Zhang & Sohn 1997). The first three orders of this model, hereafter referred to as the ZS model, can be expressed as

$$v_1^{ZS}(t) = v_1 - \tfrac{1}{8}k_1^2 v_1^2[(4A^2 + 1)v_1 t^2 + 2a_{10}t], \tag{2.2}$$

$$v_2^{ZS}(t) = -Ak_1 v_1^2 t + \tfrac{1}{6}k_1^3 v_1^2(8A^3 v_1^2 t^3 + 3Aa_{10}^2 t), \tag{2.3}$$

$$v_3^{ZS}(t) = \tfrac{3}{8}k_1^2 v_1^2[(4A^2 - 1)v_1 t^2 - 2a_{10}t], \tag{2.4}$$

where v_1 and a_{10} are the initial velocity and amplitude for the linear RMI growth, respectively. Note that the direction of the incident shock movement is considered to be the positive direction of coordinate z. Consequently, the symbols for the even-order terms are different from those used by Zhang & Sohn (1997). However, except for the variable $v_3^{ZS}(t)$, the variables $v_1^{ZS}(t)$ and $v_2^{ZS}(t)$ can receive the feedback from higher-order variables under the accuracy considered by Zhang & Sohn (1997). This may result in the divergence for predicting $v_3^{ZS}(t)$ under certain circumstances.

To characterize the perturbation growth of the multi-mode RMI, several theoretical approaches were adapted and improved from single-mode situations. For example, the ZS model was extended by Vandenboomgaerde *et al.* (2002) to predict the early nonlinear amplitude growth of multi-mode interfaces. Besides, Haan (1991) proposed a second-order solution for multi-mode classical RTI growth, which is referred to as the Haan model. The Haan model in the ordinary differential equation form for RTI growth rate can be expressed as

$$\ddot{a}_j(t) = \gamma^2 k_j\, a_j(t) + Ak_j \sum_l \left[\ddot{a}_l(t)\, a_{j-l}(t)\, (1 - \hat{\boldsymbol{k}}_l \cdot \hat{\boldsymbol{k}}_j) \right.$$

$$\left. + \dot{a}_l(t)\, \dot{a}_{j-l}(t) \left(\frac{1}{2} - \hat{\boldsymbol{k}}_l \cdot \hat{\boldsymbol{k}}_j - \frac{1}{2}\hat{\boldsymbol{k}}_l \cdot \hat{\boldsymbol{k}}' \right) \right], \tag{2.5}$$

where

$$\boldsymbol{k}' = \boldsymbol{k}_j - \boldsymbol{k}_l, \tag{2.6}$$

and $\gamma(k) = \sqrt{gkA}$ is the linear growth rate for the RTI perturbation, with g the acceleration. Here, $\boldsymbol{k}$ is the wave vector for mode k, and $\hat{\boldsymbol{k}} = \boldsymbol{k}/k$ is the unit vector. The subscripts j and l denote the corresponding modes. The first term on the right-hand side represents the contribution from the linear growth of the mode k_j itself, and the other terms represent the contribution from the second-order mode coupling between modes k_l

and k_{j-l}. Ofer *et al.* ([1996](#)) solved ([2.5](#)) under the assumption that g is a constant, and a solution for $a_j(t)$ up to second-order accuracy was given as

$$a_j(t) = a_j^{lin}(t) + \frac{1}{2}Ak_j\left(\sum_l a_l^{lin}(t)\,a_{j+l}^{lin}(t) - \frac{1}{2}\sum_{l<j} a_l^{lin}(t)\,a_{j-l}^{lin}(t)\right), \qquad (2.7)$$

where $a_j^{lin}(t)$ denotes the first-order amplitude of mode k_j, which is zero when mode k_j is not a fundamental mode. The second and third terms represent the generation of mode k_j from shorter-wavelength modes (coupling between modes k_l and k_{j+l}) and longer-wavelength modes (coupling between modes k_l and k_{j-l}), respectively. Note that ([2.5](#))–([2.7](#)) have second-order accuracy for both self-coupling and mutual coupling. If $j = 2l$, then the third term in ([2.7](#)) reduces to the first term in ([2.3](#)). Although RMI and RTI share the same linearized governing equations, whether the acceleration g equals zero or not leads to significant differences in the properties of solutions (Zhou [2017](#)). The linearized governing equation for RMI gives a linear solution (Richtmyer [1960](#)). Specifically, $a_j^{lin}(t) = a_{j0}\cosh(\gamma(k_j)\,t)$ establishes when $g \neq 0$ in the RTI situation, while $a_j^{lin}(t) = a_{j0} + v_j t$ stands when $g = 0$ in the RMI situation. The initial conditions a_{j0} and v_j are the amplitude and velocity of the mode k_j at the time when the perturbation growth enters the linear regime. Note that the derivation from ([2.5](#)) to ([2.7](#)) is not restricted to exponential growth, and ([2.7](#)) holds for RMI too. Therefore, the solutions for the mutual-coupling part of RMI can be simplified into (Remington *et al.* [1995](#))

$$a_{j\pm l}(t) \approx \mp\frac{1}{2}(k_j \pm k_l)v_j v_l t^2, \quad A \approx 1, \qquad (2.8)$$

with v_j and v_l being the linear growth rates of modes k_j and k_l, respectively. The modes $k_j \pm k_l$ are referred to as the 'beat modes' generated from the coupling between two modes k_j and k_l. Equation ([2.8](#)) equals 0 when mode k_j or k_l is not a fundamental mode. The Haan model has concise expressions and can predict the generations of beat modes.

For the dual-mode RMI (Luo *et al.* [2020](#)), the Haan model is reformulated through some mathematical treatments to obtain the weakly nonlinear solutions when the fundamental modes include k_1 and k_2:

$$v_1^{wn}(t) = v_1 + k_1 A\left(\sqrt{2}v_1 a_{20} + \tfrac{3}{2}v_1 v_2 t\right), \qquad (2.9)$$

$$v_2^{wn}(t) = v_2 - k_1 A(v_1 a_{10} + v_1^2 t), \qquad (2.10)$$

$$v_3^{wn}(t) = -\tfrac{3}{8}k_2 A[2v_1 v_2 t + v_1 a_{20} + (1 + \sqrt{2})v_2 a_{10}], \qquad (2.11)$$

$$v_4^{wn}(t) = -k_2 A(v_2^2 t + 2v_2 a_{20}). \qquad (2.12)$$

However, these weakly nonlinear solutions were derived on the premise that the exponential growth is satisfied. This may lead to an overestimation of the weakly nonlinear solutions. To suppress this overestimation, a nonlinear model proposed by Zhang & Guo ([2016](#)) for single-mode RMI (the ZG model), was introduced. The ZG model was used in previous work (Luo *et al.* [2020](#)) to suppress the nonlinear terms, because previous work (Liu *et al.* [2018](#)) has verified that the ZG model can give reasonable predictions under similar physical parameters, and can suppress the rapid growth of the mode amplitudes from the weakly nonlinear stages. However, the ZG model is not a solution to the complete perturbation problem, because it stems from a plausible closure of the solution expanded near the tip of the bubble, which may or may not provide an accurate approximation to the

actual solution. In some cases, the ZG model does not work and needs to be modified. The modified ZG model (mZG model) can be expressed as

$$v_i^{mZG}(t) = \frac{v_i^{wn}(t)}{1 + \hat{a}k_i\, v_i^{wn}(t)\, t}, \tag{2.13}$$

where $i = 1, 2, 3, 4$, and

$$\hat{a} = \frac{3}{4}\,\frac{(1+A)(3+A)}{3+A+\sqrt{2}(1+A)^{1/2}}\,\frac{4(3+A)+\sqrt{2}(9+A)(1+A)^{1/2}}{(3+A)^2+2\sqrt{2}(3-A)(1+A)^{1/2}}. \tag{2.14}$$

The Haan and mZG models are both capable of giving reasonable predictions for the evolution of RMI at a light–heavy interface. Under second-order accuracy, the divergence of these two models in late stages may be inevitable. Although the ZG model was introduced into the mZG model to suppress the overestimation, when the initial velocity is negative, the denominator of (2.13) may approach 0, which will also cause divergence.

2.2. *Asymptotic matching modal model*

We will establish a modal model based on the ideal gas equation of state for predicting the RMI development using an asymptotic matching method. After the shock impact, the amplitude growth will experience a startup process, which can be treated as a boundary layer on the time axis caused by the contradiction between the initial conditions and the linear solutions. This kind of problem can be solved by the singular perturbation method (Vasil'Eva, Butuzov & Kalachev 1995). Based on this property, the general solution $v^{gs}(t)$ can be decomposed into three parts: the internal solution $v^{in}(t)$, the external solution $v^{ex}(t)$, and the uniform approximation $v^{uni}(t)$ (Lin & Segel 1988), i.e.

$$v^{gs}(t) = v^{in}(t) + v^{ex}(t) - v^{uni}(t). \tag{2.15}$$

It is clear that the uniform approximation part is the linear growth rate. For a light–heavy interface accelerated by a weak shock wave, the impulsive model proposed by Richtmyer (1960) has been proven to provide a good prediction to the linear growth (Chen *et al.* 2023). For a heavy–light interface accelerated by a weak shock wave, the irrotational model proposed by Wouchuk and Nishihara (WN model) can give an excellent prediction for the linear growth rate (Wouchuk 2001; Li *et al.* 2024). As a result, the impulsive model and the WN model are used here to predict the linear growth rates $v^{uni}(t)$ of the light–heavy and heavy–light interfaces, respectively. The impulsive model can be written as

$$v^{imp} = ka_0^+ A\,\Delta V, \tag{2.16}$$

and the WN model can be expressed as

$$v^{WN} = ka_0^- \left[\frac{1-A}{2}\left(1+\frac{V_{RW}}{V_{IS}}\right)(U_1 - \Delta V) + \frac{1+A}{2}\left(1-\frac{V_{TS}}{V_{IS}}\right)\Delta V\right], \tag{2.17}$$

where a_0^- is the initial amplitude, $a_0^+ = (1 - \Delta V/V_{IS})a_0^-$ is the post-shock amplitude, V_{IS}, V_{TS}, V_{RW} and ΔV are the velocities of the incident shock, transmitted shock, reflected wave and shocked interface under laboratory coordinates, respectively, and U_1 is the flow velocity behind the incident shock. Given the incident shock Mach number and the physical properties of the fluids, these quantities can be solved by one-dimensional (1-D) gas dynamics theory (Anderson 1990).

The internal solution should capture the rapid acceleration of the amplitude growth immediately after the shock impact. The linear theory (Yang *et al.* 1994) or the startup process model (SP model) (Li *et al.* 2024) can be used to calculate the internal solution. The linear theory can capture the global rapid acceleration and the local vibration caused by pressure perturbations, but it has no explicit expression and must be solved numerically. The SP model has an explicit expression and can characterize the overall growth trend during the startup process. When the incident shock is not strong, and the local vibration caused by pressure perturbations is less obvious, the SP model is therefore chosen for clarity (Li *et al.* 2024). The SP model can be expressed as

$$v^{in}(t) = \frac{2v^{uni}(t)}{(1 - A) \coth[k \times L_{RW}(t)] + (1 + A) \coth[k \times L_{TS}(t)]}, \qquad (2.18)$$

where $v^{uni}(t)$ results from either (2.16) or (2.17), depending upon the interface type, and $L_{RW}(t)$ and $L_{TS}(t)$ are the distances of the reflected wave and transmitted shock from the shocked interface, which can be calculated as

$$\left.\begin{aligned} L_{RW}(t) &= (V_{RW} + \Delta V)t, \\ L_{TS}(t) &= (V_{TS} - \Delta V)t. \end{aligned}\right\} \qquad (2.19)$$

The external solution should describe the nonlinear evolution following the startup process, namely, after the amplitude reaches linear growth. At this stage, the shock is sufficiently apart from the interface and compressibility can be ignored (Zhang *et al.* 2018). Previously, the approach proposed by Haan (1991) was employed to investigate the nonlinear evolution of multi-mode RMI. However, this approach has only second-order accuracy (Haan 1991; Luo *et al.* 2020). In the present work, a perturbation expansion method is used to obtain a series solution for the external solution. One advantage of this method is that the accuracy can be controlled to any desired degree. Since the external solution should primarily capture the characteristics of incompressible nonlinear evolution in the late stage, the potential flow approach can be applied. This is done by starting from the governing equations for incompressible, inviscid, and irrotational fluids (Layzer 1955; Zhang & Sohn 1997):

$$\nabla^2 \phi_q(t, x, z) = 0, \qquad (2.20)$$

$$\frac{\partial a}{\partial t} + \frac{\partial \phi_q}{\partial x} \frac{\partial a}{\partial x} - \frac{\partial \phi_q}{\partial z} = 0 \quad \text{at } z = a, \qquad (2.21)$$

$$\sum_{q=1}^{2} (-1)^q \rho_q \left(\frac{\partial \phi_q}{\partial t} + \frac{1}{2} \left[\left(\frac{\partial \phi_q}{\partial x} \right)^2 + \left(\frac{\partial \phi_q}{\partial z} \right)^2 \right] \right) = f(t) \quad \text{at } z = a. \qquad (2.22)$$

Here, ϕ_q represents the velocity potential in fluid q, and the velocity field in fluid q is given by $\mathbf{v}_q = \nabla \phi_q$. The subscripts $q = 1, 2$ denote the fluids separated by the interface, and $z = a(x, t)$ represents the interface profile at a given time t, with x and z referring to the spanwise and normal directions of the interface, respectively. The selection of the velocity potential functions is significant for the potential flow method. By using the perturbation expansion technique, the interface and velocity potentials can be expanded into (Zhang &

Sohn 1997)

$$a(x, t) \doteq \sum_{n=1}^{N} a_n(t) \cos(nkx) = \sum_{n=1}^{N} \varepsilon^n \sum_{m=0}^{\lfloor (n+1)/2 \rfloor} a_{n,n-2m}(t) \cos(n - 2m)kx, \quad (2.23)$$

$$\phi_q(x, z, t) \doteq \sum_{n=1}^{N} \varepsilon^n \sum_{m=0}^{\lfloor (n+1)/2 \rfloor} \phi_{i,n,n-2m}(t) \exp((-1)^{q+1}(n - 2m)kz) \cos(n - 2m)kx,$$
$$(2.24)$$

where ε is the auxiliary perturbation quantity used to construct the nth-order perturbation expansion equations with dimension 1. This ε will be eliminated in the procedure and will not appear in the final expressions. In addition, The amplitude $a(x, t)$ in (2.23) is defined only at the interface, thus the far-field conditions do not exist. The potential function $\phi_q(x, z, t)$ in (2.24) is defined in the fluids on both sides of the interface. The separation of variables form of (2.24) is set to be $\exp((-1)^{q+1}(n - 2m)kz)$ for the normal direction coordinate z, which ensures that the perturbation potential diminishes far from the interface. Here, N is the expansion order of the perturbation expansion method, and the ZS model is established based on $N = 4$. The initial profile of a multi-mode interface can be expressed as

$$a^-(x) = a(x, 0^-) = \sum_j a_j^- \cos(jkx). \quad (2.25)$$

We specify the mode k_j as the fundamental mode for clarity hereafter because in the subsequent derivation, if mode k_j is not the fundamental mode, then the evolution results will degenerate to 0. The initial conditions at the nonlinear starting point for the interface can be expressed as

$$a_{n,n-2m}(t = 0) = \sum_j a_{j0} \delta_{n,j} \delta_{n-2m,j}, \quad (2.26)$$

$$v_{n,n-2m}(t = 0) = \sum_j v_j \delta_{n,j} \delta_{n-2m,j}, \quad (2.27)$$

where δ is the Kronecker symbol. The value of startup time $t = \tau$ when the perturbation evolution enters the linear growth regime can be calculated as (Lombardini & Pullin 2009; Li *et al.* 2024)

$$\tau = \frac{1}{k} \left(\frac{1 - A}{V_{RW} + \Delta V} + \frac{1 + A}{V_{TS} - \Delta V} \right). \quad (2.28)$$

Because τ relates to k, the startup times are different for fundamental modes with different wavenumbers. The treatment for different startup times will be discussed later. Here, v_j is equal to the linear growth rate, and a_{j0} in previous work has different criteria such as $(a_j^+ + a_j^-)/2$ (Zhang *et al.* 2018) or 0 (Niederhaus & Jacobs 2003). To approximate the amplitude at $t = \tau$ as much as possible, $a_{j0} = a_j^+ + v_j \tau/2$ is used in the present work since the perturbation growth at the early stage of the startup process is approximately quadratic (Lombardini & Pullin 2009). The diversity among various criteria is small when the initial amplitude is small, but may be significant when the initial amplitude is high.

Subsequently, each order of equations with a balanced order of ε can be provided, and the solutions can be derived directly. However, the expressions for the direct solutions

are very complicated. In addition, the fundamental modes have varying startup times due to their disparate wavenumbers, and the solutions for the development of the fundamental modes have disparate orders of accuracy. To overcome these difficulties, the external solution can be decomposed into two components, i.e. the self-coupling of each fundamental mode and the mutual coupling between different fundamental modes. Here we define the self-coupling of the fundamental mode k_j as the nonlinear evolution of the mode k_j itself and the generation of its integer-multiple modes of mode k_j, namely, modes $2k_j$, $3k_j$, and so on under the single mode case. Mutual coupling between two fundamental modes is the additional effect when the initial interface has more than one fundamental mode.

By considering $N = 4$, Zhang & Sohn (1997) proposed the ZS model for single-mode RMI development. The expressions for the first three modes of self-coupling of mode k_j ($j = 1$) are given by (2.2)–(2.4). As described earlier, because the feedback from high-order harmonics to the third-order harmonic is ignored, the ZS model may diverge in predicting the third-order harmonic growth. To prevent this divergence, the equation is expanded to $N = 5$ to include higher-order terms, enabling the feedback from the fifth-order harmonic to the third-order harmonic. In addition, because $ka_i \ll O(1)$, the high-order ka_i terms can be reduced for each order of t, thereby the simplified solutions can be provided. The self-coupling parts of our new model are

$$v_j^{(s)}(t) = v_j - \tfrac{1}{8}k_j^2 v_j^2[(4A^2 + 1)v_j t^2 + 2a_{j0}t], \tag{2.29}$$

$$v_{2j}^{(s)}(t) = -Ak_j v_j^2 t + \tfrac{4}{3}A^3 k_j^3 v_j^4 t^3, \tag{2.30}$$

$$v_{3j}^{(s)}(t) = -\tfrac{3}{4}k_j^2 a_{j0} v_j^2 t + \tfrac{3}{8}k_j^2 v_j^3 (4A^2 - 1)t^2$$
$$+ \tfrac{1}{32}(15 + 32A^2)k_j^4 a_{j0} v_j^4 t^3 + \tfrac{3}{128}(5 + 40A^2 - 144A^4)k_j^4 v_j^5 t^4. \tag{2.31}$$

The superscript '(s)' represents the self-coupling of a single fundamental mode. Note that our model is improved based on the ZS model. In the ZS model, only the leading term feedbacks of high-order harmonics to the first- and second-order harmonics were considered. In our model, similarly, we consider only the leading term feedbacks of high-order harmonics in the case of self-coupling, i.e. only the feedback from the third-order harmonic to the first-order harmonic is considered, and only the feedback from fifth-order harmonic to the third-order harmonic is considered. As a result, the feedback from the fifth-order harmonic is present in (2.31) but is absent in (2.29). Actually, the divergence of the nonlinear perturbation series for self-coupling is a serious issue, and a partial sum of this diverging series is not an accurate approximation to the solution. However, it is difficult to determine the number of high-order terms to achieve the best prediction. Taking k_j ($j = 1, 2$) as an example of fundamental modes combination to illustrate mutual coupling and eliminating the small quantities by scale comparison, the generations from mutual coupling are

$$v_{112}^{(m)}(t) = k_1 A v_1 v_2 t + \tfrac{1}{4}k_1^2(-2A^2 - 3)v_1 v_2^2 t^2$$
$$- \tfrac{1}{3}k_1^3(A^3 + A)v_1^3 v_2 t^3, \tag{2.32}$$

$$v_{212}^{(m)}(t) = -4A^2 v_1^2 v_2 k_1^2 t^2 + \tfrac{1}{3}(4A^3 + 5A)k_1^3 v_1^2 v_2^2 t^3$$
$$+ \tfrac{1}{24}(72A^4 + 33A^2 - 4)k_1^4 v_1^4 v_2 t^4, \tag{2.33}$$

$$v_{312}^{(m)}(t) = -3k_1 A v_1 v_2 t + \tfrac{3}{8} k_1^2 [(4A^2 - 1)v_1^2 + (-12A^2 + 1)v_2^2] v_1 t^2$$
$$+ \tfrac{1}{4} k_1^3 [(54A^3 - 11A)v_1^2 + (48A^3 + 9A)v_2^2] v_1 v_2 t^3, \qquad (2.34)$$

$$v_{412}^{(m)}(t) = k_1^2 (8A^2 - 2)v_1^2 v_2 t^2 + \tfrac{1}{3} k_1^3 (96A^3 - 28A)v_1^2 v_2^2 t^3$$
$$+ \tfrac{1}{12} k_1^4 (-512A^4 + 223A^2 + 3)v_1^4 v_2 t^4. \qquad (2.35)$$

The superscript '(m)' represents the mutual coupling between two different fundamental modes. The subscript 'ijl' denotes that the velocity of the mode k_i is generated from mutual coupling between the fundamental modes k_j and k_l. Three terms for each mode considering the mutual coupling are reserved. Series solutions with more than one term can provide convenience for further mathematical treatments such as Padé approximations. The previous studies have shown that the beat mode with wavenumber $k_j \pm k_l$ appears when more than one mode is initially present (Haan 1991; Remington *et al.* 1995; Luo *et al.* 2020). At lowest order of accuracy of time $O(t)$ and initial amplitude $O[(ka_i)^0]$, this new model can reduce to (2.7). It can be found from the new model that the other modes will also be affected by mutual coupling at higher order. This phenomenon will be verified by experiments hereinafter. By deriving a higher-accuracy model, the divergence of solutions is prevented until the profile of interface is multi-valued.

The complete form for our new model to predict the mode k_i evolution can be written as

$$v_i^{gm} = \sum_j \left\{ \left[v_i^{in}(t) - v_i^{uni} \right] \delta_{i,j} + v_i^{(s)} \left[(t - \tau_j) H(t - \tau_j) \right] + \sum_{l \neq j} v_{ijl}^{(m)} \left[(t - \tau_{jl}^{(m)}) H(t - \tau_{jl}^{(m)}) \right] \right\},$$
$$(2.36)$$

where $H(t)$ is the Heaviside function, τ_i is the time scaling for the startup process for each fundamental mode k_i, and $\tau_{jl}^{(m)} = (\tau_j + \tau_l)/2$ is the startup time of the mode generated from the mutual coupling between the fundamental modes k_j and k_l. The first term in the sum is used to match the startup process with the nonlinear growth; the second term represents the self-coupling of fundamental mode k_j, and it exists only when k_i is an integer multiple of k_j; the last term represents the mutual coupling between two different fundamental modes k_j and k_l. Note that this asymptotic matching method is not restricted to this nonlinear model, but is also applicable to other nonlinear models on RMI.

Note that the new model is established assuming that the different fundamental modes have small initial perturbation amplitudes, i.e. $ka_i \ll O(1)$, because there are existing theoretical models for predicting the linear and nonlinear growth rates of the amplitude. If the shock hits the interface with high initial perturbation amplitudes, then complicated phenomena, such as unsteady shock refraction and Mach stems, arise, and there are no analytical solutions for the linear and nonlinear growths, to the best of the authors' knowledge. In the present work, the relative phase difference of two different fundamental modes should be integer multiples of π, such that the dual-mode interface can be expressed in the form $z = a_{01} \cos(k_1 x) \pm a_{02} \cos(k_2 x)$. For high-frequency multi-mode initial conditions (with fundamental modes greater than 2), provided that the relative phase differences of the different fundamental modes are integer multiples of π, the different startup processes of the different fundamental modes can still be captured by the asymptotic matching method proposed, and (2.36) still holds. Besides, the perturbation expansion method for nonlinear evolution can still be applied although the specific expressions for the nonlinear part are different.

In addition, the new model should be effective for a wide range of Atwood numbers as it is derived directly from potential flow models without empirical parameters and has a

series form of Atwood number, but it may lose validity at extreme Atwood numbers such as $|A| < 0.1$ or $|A| > 0.9$. For light–heavy interfaces, the model may be applicable only for low shock Mach numbers because the shock proximity effect will significantly flatten the bubble front when the incident shock is strong (Motl *et al.* 2009). The change in the bubble morphology will alter the modal evolution, which affects the validity of the model. For heavy–light interfaces, since the transmitted shock wave will quickly move away from the interface due to the high acoustic velocity of the fluid on the transmitted side, the shock proximity effect is very weak, and the model is expected to be effective for relatively high Mach numbers.

To verify the model proposed, experiments are performed. Note that very limited data are available on the startup process in the literature. Moreover, RMI of a dual-mode heavy–light interface has never been considered previously. Consequently, both single-mode and dual-mode interfaces are considered, and both light–heavy and heavy–light interfaces are involved in our present experiments. In the following, experimental methods and results are first described and discussed, then comparison of experimental results with theoretical results is made.

3. Experimental methods

In experiments, five different interface profiles are designed, including three kinds of single-mode interface with different wavenumbers, and two kinds of dual-mode interface with different phase combinations. The profiles of the initial interfaces can be expressed as

$$
\left.
\begin{array}{lll}
\text{SM\_lh} & z = a_{01}\cos(k_1 x), & x \in [0, 120]\,\text{mm}, \\
\text{SM\_hl} & z = -a_{01}\cos(k_1 x), & x \in [-30, 90]\,\text{mm}, \\
\text{AP\_lh} & z = a_{01}\cos(k_1 x) - a_{02}\cos(k_2 x), & x \in [-90, 30]\,\text{mm}, \\
\text{IP\_lh} & z = a_{01}\cos(k_1 x) + a_{02}\cos(k_2 x), & x \in [-60, 60]\,\text{mm}, \\
\text{AP\_hl} & z = -a_{01}\cos(k_1 x) + a_{02}\cos(k_2 x), & x \in [-30, 90]\,\text{mm}, \\
\text{IP\_hl} & z = -a_{01}\cos(k_1 x) - a_{02}\cos(k_2 x), & x \in [-60, 60]\,\text{mm},
\end{array}
\right\}
\tag{3.1}
$$

where k_1 and k_2 are wavenumbers of two fundamental modes, and a_{01} and a_{02} are initial amplitudes of two fundamental modes at the boundary plane. Note that the initial negative amplitude of the mode k_1 in dual-mode heavy–light cases is designed to maintain a positive velocity. The width of the flow field is 140 mm, consisting of perturbation with two to four periods and two straight segments on both sides to eliminate the boundary effects (Luo *et al.* 2018). For each interface configuration, both air–SF_6 and SF_6–air interfaces are involved.

The soap-film technique (Liu *et al.* 2018; Gao *et al.* 2024) is used to form the discontinuous interfaces in this work. The super-hydrophobic-oleophobic surface technique developed by Li *et al.* (2023) instead of filaments is used to constrain the soap-film interface. Due to the surface tension, the soap-film interface is a 3-D surface with a minimum-surface feature (Luo, Wang & Si 2013). The multi-mode 3-D surface can be expressed as

$$
z = \sum_j f_j(y)\cos(k_j x). \tag{3.2}
$$

When only one fundamental mode exists, the interface reduces to a single-mode one, and the governing function for $f_j(y)$, according to the work of Luo *et al.* (2013), is

$$
f_j'' = k^2 f_j(1 + f_j'^2), \quad f_j'|_{y=0} = 0, \quad f_j|_{y=0} = a_j^{sp}, \tag{3.3a–c}
$$

1002 A16-11

Case	λ_1	a_{01}	a_{v1}	λ_2	a_{02}	a_{v2}	a	a_b	a_s	θ_b	θ_s
SM30_hl	30	1	0.89	—	—	—	0.89	0.89	0.89	π	0
SM40_hl	40	1.33	1.24	—	—	—	1.24	1.24	1.24	π	0
SM60_hl	60	2	1.94	—	—	—	1.94	1.94	1.94	π	0
AP_lh	60	2	1.94	30	1	0.89	2.12	1.42	2.82	0.32π	π
IP_lh	60	2	1.94	30	1	0.89	2.12	2.82	1.42	0	0.68π
AP_hl	60	2	1.94	30	1	0.89	2.12	1.42	2.82	0.68π	0
IP_hl	60	2	1.94	30	1	0.89	2.12	2.82	1.42	π	0.32π

Table 1. Initial interface parameters, where '_lh' or '_hl' indicate that the interfaces are light–heavy or heavy–light, respectively. For single-mode cases, the parameters for light–heavy and heavy–light interfaces are the same except for θ_b and θ_s. For a light–heavy interface, $\theta_b = 0$ and $\theta_s = \pi$. Also, 'AP' and 'IP' denote anti-phase and in-phase of two basic modes, λ is the perturbation wavelength, a_0 is the perturbation amplitude on the constraint boundary, and a_v is the integral average amplitude of the 3-D surface. The subscripts 1 and 2 denote the first and second basic modes on the initial interface, a_b, a_s, a are the initial heights of the bubble, spike and amplitude, respectively, and θ_b and θ_s are the angular locations of bubble and spike. The unit of length is mm.

where a_j^{sp} is the perturbation amplitude of the fundamental mode k_j at the symmetry plane $y = 0$. Note that (3.3a–c) is a homogeneous ordinary differential equation, and each $f_j(y)$ should satisfy (3.3a–c) for a multi-mode interface. For different fundamental modes in a multi-mode soap-film interface, the 3-D effect is different, therefore the 3-D correction of the perturbation amplitude is obligatory. The average amplitude of the fundamental mode k_j is calculated by

$$a_{vj} = \frac{\int_{-h/2}^{h/2} f_j(y)\,dy}{h}. \tag{3.4}$$

The initial interface parameters, including the average amplitudes of the fundamental modes, are provided in table 1.

The experiments are conducted in a horizontal shock tube (Guo *et al.* 2022). For air–SF$_6$ interfaces, the Mach number of the incident shock moving in air is 1.26 ± 0.01. For SF$_6$–air interfaces, the Mach number of the incident shock moving in SF$_6$ is 1.31 ± 0.01. The physical parameters of the background flow of ten cases are listed in table 2. The experimental measurements agree well with the theoretical calculations from 1-D theory. The post-shock flow is recorded by high-speed schlieren photography. The frame rate of the high-speed video camera (FASTCAM SA-Z, Photron Limited) is $50\,000$ frames per second, and the exposure time is $1/2\,880\,000$ s. The spatial resolution of the schlieren image is 0.26 ± 0.01 mm pixel^{-1}. The ambient pressure and temperature are 101.3 ± 0.1 kPa and 297.5 ± 0.7 K, respectively.

4. Results and discussion

4.1. *Qualitative results*

Developments of wave patterns and interface morphologies of the shock-accelerated air–SF$_6$ interfaces and SF$_6$–air interfaces obtained from experiments are shown in figures 1 and 2, respectively. The time origin $t = 0$ is defined as the moment when the transmitted shock wave leaves the interface. When the interface and waves are away from the initial

Interface type	Case	Ma	V_{IS}	ψ	ΔV^e	ΔV^{1-D}	V_{TS}^e	V_{TS}^{1-D}	A
Light–heavy	SM30	1.26	435.5	98 %	92.1	88.9	192.6	192.3	0.70
	SM40	1.26	436.8	99 %	91.3	89.6	195.1	191.6	0.70
	SM60	1.26	436.2	99 %	92.1	89.1	194.3	191.2	0.70
	AP	1.26	435.5	98 %	92.1	89.2	195.1	191.7	0.70
	IP	1.26	435.5	97 %	90.4	88.9	192.6	192.3	0.70
Heavy–light	SM30	1.31	179.75	98 %	96.9	95.0	403.78	407.44	−0.68
	SM40	1.32	180.28	99 %	99.4	96.8	406.93	408.73	−0.69
	SM60	1.30	177.04	100 %	96.0	92.1	405.31	405.51	−0.69
	AP	1.30	181.58	96 %	96.7	96.0	408.03	408.13	−0.68
	IP	1.31	179.47	99 %	95.0	96.0	405.74	408.14	−0.69

Table 2. Physical parameters of background flow: Ma is the incident shock Mach number, ψ is the volume fraction of SF_6 on the heavy gas side of the interface, and V_{IS}, ΔV and V_{TS} are the velocities of the incident shock, shocked interface and transmitted shock, respectively. The superscripts e and $1\text{-}D$ denote the data obtained from experimental measurements and 1-D gas dynamics theory, respectively. The unit of velocity is $\mathrm{m\,s}^{-1}$.
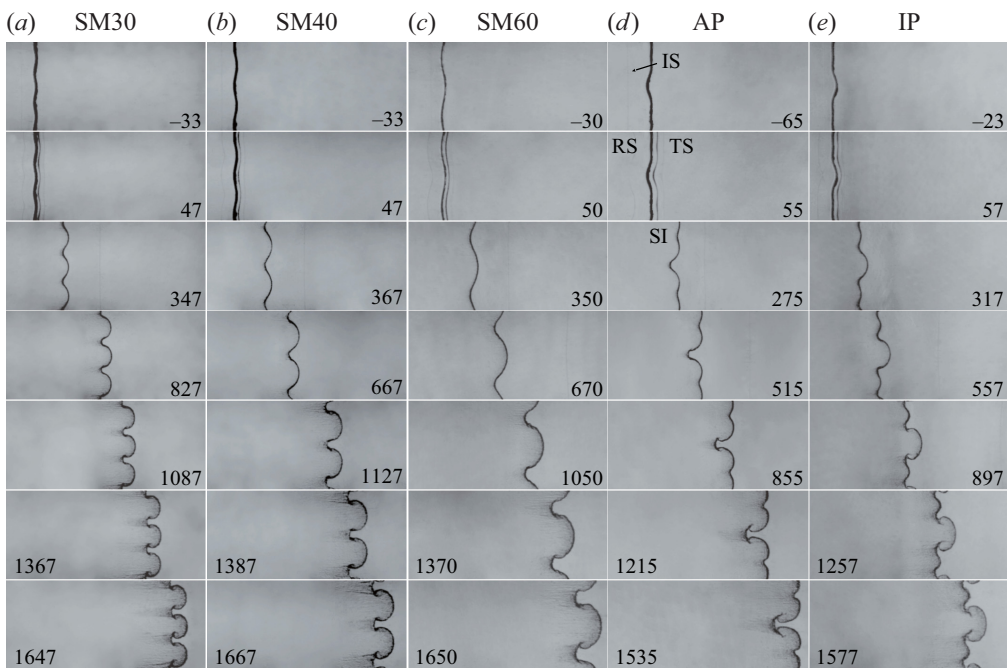

Figure 1. Sequences of schlieren images of air–SF_6 interface evolution and wave propagation for five cases: (a–c) single-mode interfaces, (d,e) dual-mode interfaces. Here, IS means incident shock, RS means reflected shock, TS means transmitted shock, and SI means shocked interface.

position, the shadows of the initial interface are erased from experimental images for clarity.

The developments of a single-mode air–SF_6 interface and SF_6–air interface accelerated by a planar shock have been widely investigated, and only a brief description is provided here. Taking case SM40 as an example, after the incident shock passes through the air–SF_6 interface, as shown in figure 1, the perturbation amplitude begins to grow, and the spikes
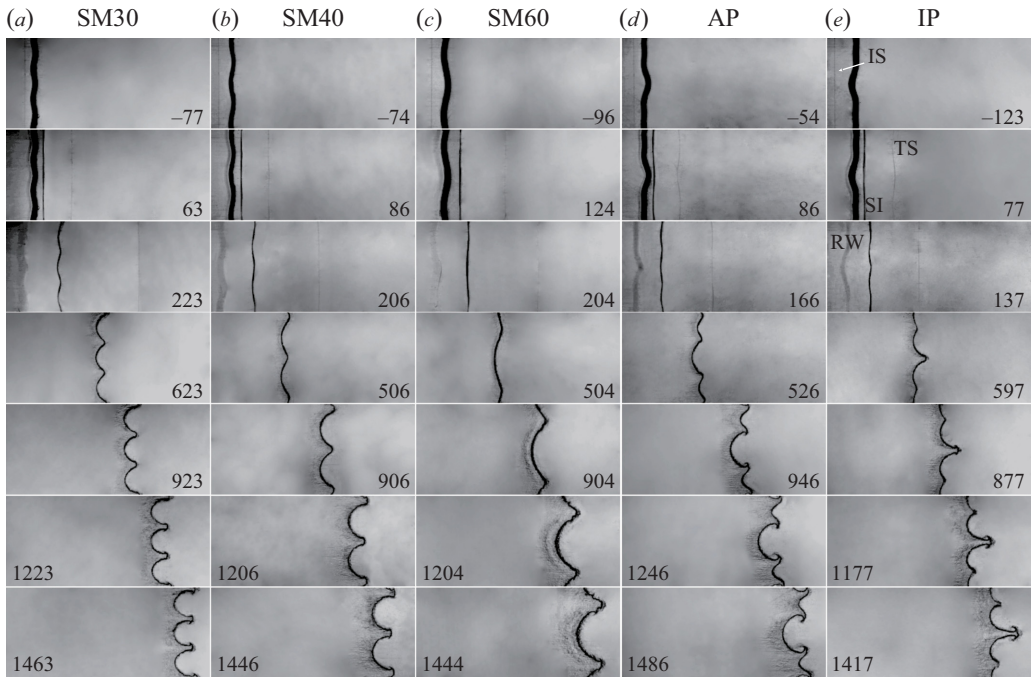
Figure 2. Sequences of schlieren images of SF_6–air interface evolution and wave propagation for five cases: (*a–c*) single-mode interfaces, (*d,e*) dual-mode interfaces.

(heavier fluid penetrating lighter fluid) and bubbles (lighter fluid penetrating heavier fluid) arise quickly ($t = 1127\,\mu s$). At the late stages, vortices are generated on both sides of the spikes ($t = 1667\,\mu s$). For a shock-accelerated SF_6–air interface, as shown in figure 2, after the shock impact, reflected rarefaction waves (RW) are clearly observed, and become wider in width ($t = 86$–$206\,\mu s$). No additional reflected waves are generated benefiting from the new interface formation method. The shocked interface experiences a phase inversion, then develops continuously. Later, vortices also arise at the spike head ($t = 1446\,\mu s$).

For the dual-mode interfaces, we take case AP as an example to detail the process. The air–SF_6 interface in figure 1 has a large spike at the centre and small ones located on both sides. After the shock wave accelerates the interface, the large spike rolls up with a pair of vortices formed at its neck, and bubbles develop with an obvious inclination to the large spike ($t = 855\,\mu s$). At late times, the difference between the sizes of the different spikes becomes more significant, but the interface profile remains relatively thin and distinct ($t = 1535\,\mu s$). The SF_6–air interface in figure 2 has a large bubble at the centre and small ones located on both sides. Because different fundamental modes have different phase-inversion times, a moment when the amplitude reduces to zero does not exist. The mode with a short wavelength finishes phase inversion earlier, and the interface appears to be a single-mode one with $\lambda = 60\,mm$ ($t = 86\,\mu s$). Then the mode with a long wavelength finishes phase inversion, causing the dual-mode interface to resemble a single-mode interface with $\lambda = 30\,mm$ ($t = 166\,\mu s$). Later, both large and small bubbles appear on the interface ($t = 526\,\mu s$), and the small spikes develop with an apparent inclination to the large bubble ($t = 946\,\mu s$).

To perform modal analysis, in the previous work, Fourier analysis on the interface profile is made. However, for each x pixel, we will choose a certain single z pixel during the data
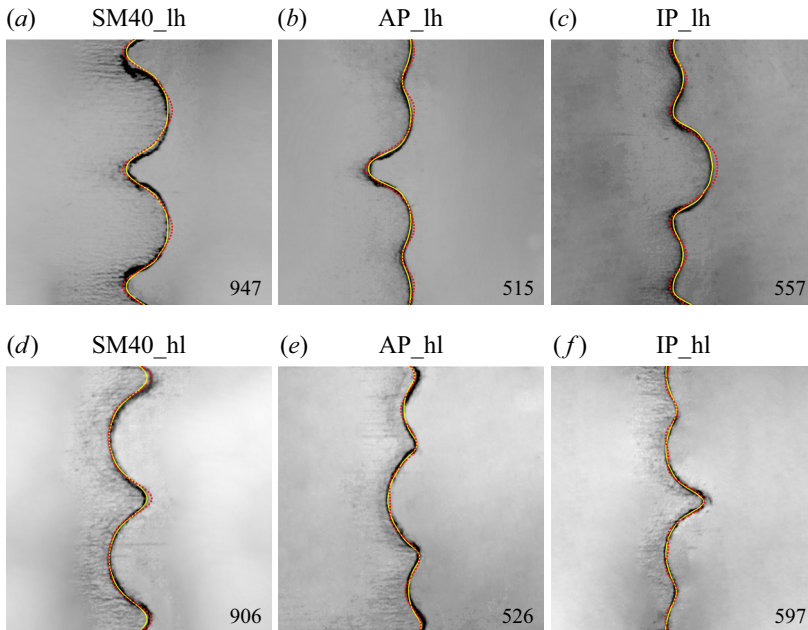
1002 A16-14

Figure 3. Comparisons between experimental schlieren images and interface profiles extracted from mode decomposition (solid lines) and theoretical prediction (dotted lines).

processing since Fourier analysis is executed on a single-valued function, and only one period of the interface is involved. In the present work, the cosine series function is used to fit the experimental profiles using the nonlinear least squares method. This method allows us to retain all the dark pixels near the interface during the binarization process rather than choosing an individual pixel for each x coordinate. In addition, this procedure can be conducted over the whole observation area rather than for a single period. Therefore, more information from the experimental images is utilized, and the human subjectivity is reduced. A remarkable advantage of the modal model is that the direct profile of the interface can be predicted, whereas the other models based on a selected linear start point cannot give this prediction. Figure 3 shows comparisons between the experimental schlieren images and the interface profiles extracted from mode decomposition and predicted from the theoretical model for different cases. From comparison, the modal model can predict the profile very well, although some small localized features cannot be predicted due to the ignorance of higher-order harmonics in the model.

4.2. *Quantitative comparisons*

To verify our model, comparisons of the amplitude variations between experimental measurements and theoretical predictions from the new model for single-mode cases are given in dimensionless form in figure 4. Note that as the small-amplitude asymptotic RMI growth rate is itself proportional to the initial ripple amplitude, by the time the startup process ends, we need to ensure that the linear theory is still applicable, i.e. the small-amplitude conditions should be satisfied. For light–heavy interfaces, perturbation amplitudes will continue to grow after the shock impact. The amplitude (a_i) at the time of the startup process ending ($t = \tau_i$) will be larger than the value at the initial time. For heavy–light interfaces, however, due to the presence of the phase-inversion process,
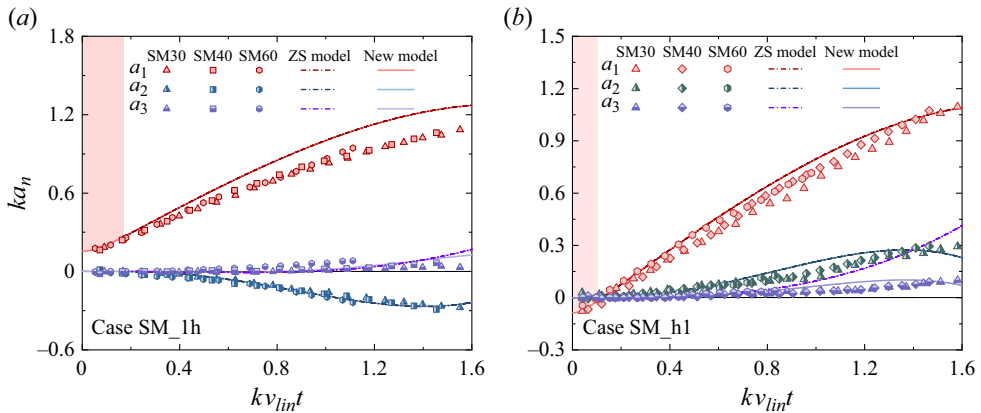
Figure 4. Comparisons of the normalized amplitude developments between experimental measurements and theoretical predictions for single-mode cases. The pink zone indicates the startup process of the fundamental mode.

the amplitude will first reduce and then grow in the opposite phase, which leads to $|a_i(t = \tau_i)| < |a_i(t = 0)|$. In our present single-mode and dual-mode experiments, the dimensionless amplitude of each fundamental mode after the startup process $|ka_i(t = \tau_i)| < 0.3$ holds. Under this condition, the high-amplitude effect is negligible for the linear and nonlinear growths of both light–heavy and heavy–light interfaces (Dimonte & Ramaprabhu 2010; Wang *et al.* 2023*a*), and linear theory is still valid to provide a linear growth rate. Therefore, the small-amplitude conditions hold for the nonlinear modal evolution in our experiments. The amplitudes of the first three harmonics are provided since the amplitudes of other higher-order harmonics are too small. The time and *n*th-order harmonic amplitude are normalized as $kv_{lin}t$ and ka_n, respectively, where v_{lin} is the linear growth rate of the total perturbation amplitude, which can be calculated by

$$v_{lin} = \sum_j [v_j \cos(j\theta_s) - v_j \cos(j\theta_b)]/2, \tag{4.1}$$

where θ_b and θ_s are the phase positions of the bubble and spike, respectively, as listed in table 1. Benefiting from the asymptotic matching model, the development of harmonic amplitude can be predicted from the moment when the shock impact is finished, namely $t = 0$, rather than from an artificially selected startup time. Note that the ZS model cannot predict the startup process, and the start point of the prediction by the ZS model is given by our new model. As mentioned before, relative to the ZS model, the correction is made only to the third harmonic in the new model. Therefore, for the amplitude growths of the first and second harmonics, the new model provides predictions similar to those of the ZS model. One can observe some obvious differences regarding normalized a_1 between experiments and theoretical predictions in light–heavy cases. Previous works have verified that the ZS model slightly overestimates the evolution of a_1 in single-mode situations with Atwood number smaller than 0.75 (Liu *et al.* 2018; Chen *et al.* 2023), generally because the amplitude growth rate predicted by the ZS model satisfies a $1/t^2$ law when the Atwood number is smaller than 0.75, but the late-time $1/t$ law of the amplitude growth rate is expected from the potential flow model, and has been validated in previous numerical and experimental works (Dimonte & Ramaprabhu 2010; Mansoor *et al.* 2020). The early overestimation results in the divergence of the ZS model in predicting a_1. In figure 4,

1002 A16-16

the predictions to the amplitude growth of the third harmonic from the ZS model and the new model are provided for comparison. For an air–SF_6 interface, the predictions from the ZS model and the new model almost coincide except in the late stages. For SF_6–air interfaces, the phase-inversion process can be well predicted by the model. For the third-order harmonic, the prediction from the ZS model coincides with the prediction from the new model before $kv_{lin}t = 0.8$. Afterwards, the prediction from the ZS model diverges, whereas the new model can still give a reasonable prediction.

Note that in the derived model, the divergence is well inhibited in the late stages by considering the fifth-order feedback to the third-order harmonic evolution. It is also possible for considering higher-order feedback to the higher-order (larger than 3) harmonic evolution, but it may not be meaningful. First and most importantly, the present modal model can already reasonably describe the profile evolution of the interface before the interface enters a non-single-valued period, and it is not necessary to consider more high-order harmonics. Second, the mathematical treatment becomes quite complicated if higher-order feedback to the higher-order (larger than 3) harmonic evolution is considered without obviously improving the accuracy. For further analysis of multi-mode perturbation fingers, it may be more effective to apply Padé approximations than higher-order expansion.

Comparisons of the amplitudes of the first four harmonics between experimental measurements and theoretical predictions for dual-mode cases are given in figure 5. The dimensionless time is shorter than that in single-mode cases because the interface enters a multi-valued period earlier. Here, the predictions from the Haan model (Haan 1991) and from the mZG model (Luo *et al.* 2020) are provided as references, and they start from the end of the startup process, i.e. from $t = \tau$, whereas the predictions from the new model start from $t = 0$. Note that the same asymptotic method is applied for our model as for the previous models. For air–SF_6 interfaces, the predictions for the first harmonic from the new model are less accurate than those from the mZG model, which is probably ascribed to the overestimation of the ZS model to the first harmonic. Nevertheless, the new model generally gives good predictions to the amplitude developments of first four harmonics, especially for the high-order harmonics. For SF_6–air interfaces, the new model provides better predictions to the amplitude developments of the first four harmonics than the other two models. Specifically, the different phase-inversion times for different fundamental modes are also well captured by the new model, which is never considered in the previous models, to the best of our knowledge. Note that the fourth-order harmonic is not the beat mode, therefore the Haan model cannot capture the mutual-coupling effect on the amplitude evolution of the fourth-order harmonic. In the Haan model, the fourth-order harmonic comes from the self-coupling of the fundamental second mode. Consequently, the Haan model gives the same results for the amplitude growths of the fourth-order harmonic in AP and IP cases. However, the amplitude growths of the fourth-order harmonic in AP and IP cases are obviously different in experiments. This fact shows that the mutual-coupling effect cannot be ignored when predicting the amplitude growth of the fourth-order harmonic, and the new model is able to quantify this effect.

As for the mZG model (Luo *et al.* 2020), the amplitude growth rates of the third- and fourth-order harmonics can be calculated using (2.13) and (2.14). Here, when the fundamental modes are k_j ($j = 1, 2$), the third- and fourth-order expressions for the weakly nonlinear solutions to initiate the mZG model are given by (2.11) and (2.12). Note that the mZG model provides different initial velocities for the amplitude growths of the third- and
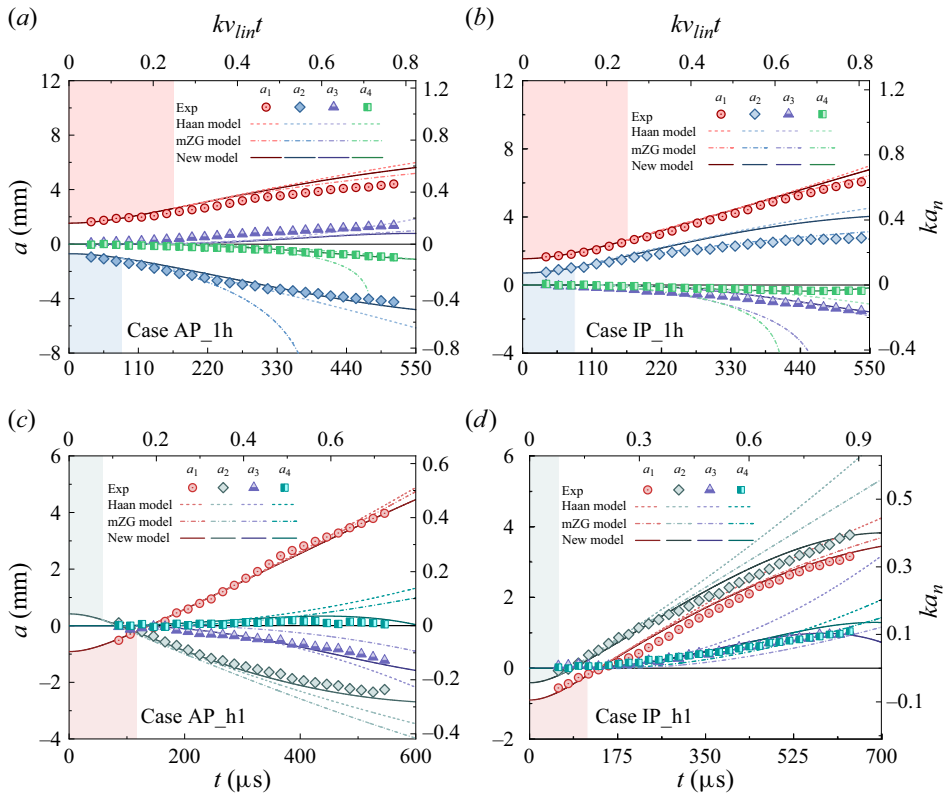
Figure 5. Comparisons of the amplitude developments between experimental measurements and theoretical predictions for dual-mode interfaces. The coloured zones indicate the startup processes of the fundamental modes.

fourth-order harmonics compared to the early evolution trends of experimental results. For example, when the two fundamental modes of the dual-mode heavy–light interface are in phase, the initial velocity calculated by (2.11) is negative, while the initial velocities predicted by the Haan model and our new model are both zero. This is because the weakly nonlinear solution for the mZG model is based on the RTI frame, which leads to an artificial initial velocity for higher-order harmonics generated from mutual coupling. However, the linearized governing equation for the RMI problem is a homogeneous ordinary differential equation, which means that the RMI problem within the linear regime satisfies the linear superposition principle. Namely, the higher-order harmonics generated from mutual coupling do not own their initial velocities. This is also consistent with the experimental results and theoretical predictions from the Haan model and the new model.

5. Conclusions

For a shock-accelerated single-mode interface, previous works have shown that there is a startup process before the amplitude growth enters the linear and nonlinear regimes. In particular, there is a phase-inversion process for a shock-accelerated heavy–light interface. Previous models were generally established based on an artificially selected initial conditions to predict the linear and nonlinear growth rates. The startup process and

the phase-inversion process cannot be described by the models. If multiple fundamental modes are present on the initial interface, then the startup times and phase-inversion times are distinct for different fundamental modes, which bring about more challenges for the model to predict each mode evolution.

In this work, an asymptotic matching modal model was established for predicting mode evolution in single- and dual-mode interfaces accelerated by a shock wave. The key to establishing the new model is the treatment of the startup process. The startup process can be treated as a boundary layer on the time axis caused by the contradiction between the initial conditions and the linear solutions. This kind of problem can be solved by the singular perturbation method. By decomposing the general solution into three parts – i.e. the internal solution, external solution and the uniform approximation – a modal model that can characterize the complete evolution of the perturbed interface after the shock impact is established. In the new model, the diverse startup times of the fundamental modes and higher-order harmonics are considered by asymptotically matching the nonlinear evolution of each mode separately. Relative to the previous modal model proposed by Haan (1991), in which only one term is reserved, three terms for each mode generated from mode coupling are reserved in the new model, which provides a convenience for further mathematical treatments. To the best of the authors' knowledge, the new model can characterize the complete evolution of various-order modes for single- and multi-mode perturbations, whereas the previous models cannot. In addition, the asymptotic matching method established in this work is not restricted to the new model but is also applicable to other nonlinear models.

To validate the model, experiments on the developments of single- and dual-mode interfaces accelerated by a shock wave are conducted, and both light–heavy and heavy–light interfaces are involved. To obtain the interface profiles, the cosine series function is used to fit the experimental profile using the nonlinear least squares method. This method allows for utilizing more information from the experimental images, and reduces the human subjectivity. The interface profiles extracted from mode decomposition and predicted by the new model show high consistency with the experimental schlieren images.

For the shocked single-mode interface evolution, the ZS model (Zhang & Sohn 1997) predicts the amplitude growth from the end of the startup process. The ZS model contains higher-order feedback only to the first- and second-order harmonics, which leads to the divergence in predicting the third-order harmonic evolution in the late stages. This divergence is well inhibited by considering the fifth-order feedback to the third-order harmonic evolution in the new model. For the shocked dual-mode interface evolution, the new model provides thorough solutions and characterizes the diverse startup times and phase inversion times for different fundamental modes for the first time. Relative to the modal model proposed by Haan (1991), the new model has a higher-order accuracy, and can evaluate the effect of mutual coupling between the fundamental modes on the amplitude variations of higher-order harmonics besides the 'beat modes'. Relative to the mZG model (Luo *et al.* 2020), the new model provides better predictions to the amplitude growths of the first four harmonics for the heavy–light interfaces, because the mZG model provides inappropriate velocities to initiate the developments of the higher-order harmonics, and gives completely different growth trends due to the presence of the phase-inversion process.

However, the present experiments were conducted only with weakly incident Mach number 1.2–1.3 and specific gas combinations of air and SF_6 to validate the new model. In future work, more experiments, including different shock Mach numbers, different

gas combinations, and more fundamental modes (greater than two) existing at the initial interface, will be conducted to further verify the new model.

Author ORCIDs.

Jiaxuan Li https://orcid.org/0009-0004-7672-3624;

Zhigang Zhai https://orcid.org/0000-0002-0094-5210;

Xisheng Luo https://orcid.org/0000-0002-4303-8290.

REFERENCES

ANDERSON, J.D. 1990 *Modern Compressible Flow: With Historical Perspective*. McGraw-Hill.
CHAPMAN, P.R. & JACOBS, J.W. 2006 Experiments on the three-dimensional incompressible Richtmyer–Meshkov instability. *Phys. Fluids* **18**, 074101.
CHEN, C., XING, Y., WANG, H., ZHAI, Z. & LUO, X. 2023 Experimental study on Richtmyer–Meshkov instability at a light–heavy interface over a wide range of Atwood numbers. *J. Fluid Mech.* **975**, A29.
CHEN, Q., LI, L., ZHANG, Y. & TIAN, B. 2019 Effects of the Atwood number on the Richtmyer–Meshkov instability in elastic–plastic media. *Phys. Rev.* E **99**, 053102.
CHU, Y., WANG, Z., QI, J., XU, Z. & LI, Z. 2022 Numerical performance assessment of double-shell targets for Z-pinch dynamic hohlraum. *Matt. Radiat. Extrem.* **7**, 035902.
COBOS CAMPOS, F. & WOUCHUK, J.G. 2014 Analytical asymptotic velocities in linear Richtmyer–Meshkov-like flows. *Phys. Rev.* E **90**, 053007.
COBOS CAMPOS, F. & WOUCHUK, J.G. 2016 Analytical scalings of the linear Richtmyer–Meshkov instability when a shock is reflected. *Phys. Rev.* E **93**, 053111.
DI STEFANO, C., RASMUS, A., DOSS, F., FLIPPO, K., HAGER, J., KLINE, J. & BRADLEY, P. 2017 Multimode instability evolution driven by strong, high-energy-density shocks in a rarefaction-reflected geometry. *Phys. Plasmas* **24**, 052101.
DIMONTE, G., NAGORI, M., RAMAPRABHU, P. & BOUREIMA, I. 2024 Simulations and models for the Richtmyer–Meshkov instability with broadband perturbations. *Phys. Fluids* **36**, 025143.
DIMONTE, G. & RAMAPRABHU, P. 2010 Simulations and model of the nonlinear Richtmyer–Meshkov instability. *Phys. Fluids* **22**, 014104.
ELBAZ, Y. & SHVARTS, D. 2018 Modal model mean field self-similar solutions to the asymptotic evolution of Rayleigh–Taylor and Richtmyer–Meshkov instabilities and its dependence on the initial conditions. *Phys. Plasmas* **25**, 062126.
FRALEY, G. 1986 Rayleigh–Taylor stability for a normal shock wave-density discontinuity interaction. *Phys. Fluids* **29**, 376–386.
GAO, X., GUO, X., ZHAI, Z. & LUO, X. 2024 Interfacial instabilities driven by co-directional rarefaction and shock waves. *J. Fluid Mech.* **980**, A20.
GE, J., LI, H., ZHANG, X. & TIAN, B. 2022 Evaluating the stretching/compression effect of Richtmyer–Meshkov instability in convergent geometries. *J. Fluid Mech.* **946**, A18.
GUO, X., CONG, Z., SI, T. & LUO, X. 2022 Shock-tube studies of single- and quasi-single-mode perturbation growth in Richtmyer–Meshkov flows with reshock. *J. Fluid Mech.* **941**, A65.
HAAN, S.W. 1991 Weakly nonlinear hydrodynamic instabilities in inertial fusion. *Phys. Fluids* B **3**, 2349–2355.
HURRICANE, O.A., PATEL, P.K., BETTI, R., FROULA, D.H., REGAN, S.P., SLUTZ, S.A., GOMEZ, M.R. & SWEENEY, M.A. 2023 Physics principles of inertial confinement fusion and US program overview. *Rev. Mod. Phys.* **95**, 025005.
LAYZER, D. 1955 On the instability of superposed fluids in a gravitational field. *Astrophys. J.* **122**, 1.
LI, J., CAO, Q., HE, W., ZHAI, Z. & LUO, X. 2023 New interface formation method for shock–interface interaction studies. *Exp. Fluids* **64**, 170.
LI, J., CHEN, C., ZHAI, Z. & LUO, X. 2024 Effects of compressibility on Richtmyer–Meshkov instability of heavy/light interface. *Phys. Fluids* **36** (5), 056104.
LIANG, Y. & LUO, X. 2023 Review on hydrodynamic instabilities of a shocked gas layer. *Sci. China Phys. Mech. Astron.* **66**, 104701.

LIN, C. & SEGEL, L. 1988 *Mathematics Applied to Deterministic Problems in the Natural Sciences*. SIAM.

LIU, C., ZHANG, Y. & XIAO, Z. 2023 A unified theoretical model for spatiotemporal development of Rayleigh–Taylor and Richtmyer–Meshkov fingers. *J. Fluid Mech.* **954**, A13.

LIU, L., LIANG, Y., DING, J., LIU, N. & LUO, X. 2018 An elaborate experiment on the single-mode Richtmyer–Meshkov instability. *J. Fluid Mech.* **853**, R2.

LOMBARDINI, M. & PULLIN, D.I. 2009 Startup process in the Richtmyer–Meshkov instability. *Phys. Fluids* **21**, 044104.

LUO, X., GUAN, B., SI, T., ZHAI, Z. & WANG, X. 2016 Richtmyer–Meshkov instability of a three-dimensional SF_6–air interface with a minimum-surface feature. *Phys. Rev.* E **93** (7), 013101.

LUO, X., LI, M., DING, J., ZHAI, Z. & SI, T. 2019 Nonlinear behaviour of convergent Richtmyer–Meshkov instability. *J. Fluid Mech.* **877**, 130–141.

LUO, X., LIANG, Y., SI, T. & ZHAI, Z. 2018 Effects of non-periodic portions of interface on Richtmyer–Meshkov instability. *J. Fluid Mech.* **861**, 309–327.

LUO, X., LIU, L., LIANG, Y., DING, J. & WEN, C. 2020 Richtmyer–Meshkov instability on a dual-mode interface. *J. Fluid Mech.* **905**, A5.

LUO, X., WANG, X. & SI, T. 2013 The Richtmyer–Meshkov instability of a three-dimensional air/SF_6 interface with a minimum-surface feature. *J. Fluid Mech.* **722**, R2.

MANSOOR, M., DALTON, S., MARTINEZ, A., DESJARDINS, T., CHARONKO, J. & PRESTRIDGE, K. 2020 The effect of initial conditions on mixing transition of the Richtmyer–Meshkov instability. *J. Fluid Mech.* **904**, A3.

MESHKOV, E.E. 1969 Instability of the interface of two gases accelerated by a shock wave. *Fluid Dyn.* **4**, 101–104.

MEYER, K.A. & BLEWETT, P.J. 1972 Numerical investigation of the stability of a shock-accelerated interface between two fluids. *Phys. Fluids* **15**, 753–759.

MOTL, B., OAKLEY, J., RANJAN, D., WEBER, C., ANDERSON, M. & BONAZZA, R. 2009 Experimental validation of a Richtmyer–Meshkov scaling law over large density ratio and shock strength ranges. *Phys. Fluids* **21**, 126102.

NIEDERHAUS, C.E. & JACOBS, J.W. 2003 Experimental study of the Richtmyer–Meshkov instability of incompressible fluids. *J. Fluid Mech.* **485**, 243–277.

OFER, D., ALON, U., SHVARTS, D., MCCRORY, R. & VERDON, C. 1996 Modal model for the nonlinear multimode Rayleigh–Taylor instability. *Phys. Plasmas* **3**, 3073–3090.

PRESTRIDGE, K. 2018 Experimental adventures in variable-density mixing. *Phys. Rev. Fluids* **3** (15), 110501.

RAYLEIGH, LORD 1882 Investigation of the character of the equilibrium of an incompressible heavy fluid of variable density. *Proc. Lond. Math. Soc.* **1**, 170–177.

REMINGTON, B., WEBER, S., MARINAK, M., HAAN, S., KILKENNY, J., WALLACE, R. & DIMONTE, G. 1995 Single-mode and multimode Rayleigh–Taylor experiments on Nova. *Phys. Plasmas* **2**, 241–255.

RICHTMYER, R.D. 1960 Taylor instability in shock acceleration of compressible fluids. *Commun. Pure Appl. Maths* **13**, 297–319.

SCHALLES, M. 2023 Experiments on the three-layer Richtmyer–Meshkov instability. Master's thesis, University of Arizona.

TAYLOR, G. 1950 The instability of liquid surfaces when accelerated in a direction perpendicular to their planes. I. *Proc. R. Soc. Lond.* A **201**, 192–196.

VANDENBOOMGAERDE, M., GAUTHIER, S. & MÜGLER, C. 2002 Nonlinear regime of a multimode Richtmyer–Meshkov instability: a simplified perturbation theory. *Phys. Fluids* **14**, 1111–1122.

VASIL'EVA, A., BUTUZOV, V. & KALACHEV, L. 1995 *The Boundary Function Method for Singular Perturbation Problems*. SIAM.

WANG, H., WANG, H., ZHAI, Z. & LUO, X. 2023*a* High-amplitude effect on Richtmyer–Meshkov instability at a single-mode heavy–light interface. *Phys. Fluids* **35**, 126107.

WANG, H., WANG, H., ZHAI, Z. & LUO, X. 2023*b* High-amplitude effect on single-mode Richtmyer–Meshkov instability of a light–heavy interface. *Phys. Fluids* **35**, 016106.

WOUCHUK, J.G. 2001 Growth rate of the Richtmyer–Meshkov instability when a rarefaction is reflected. *Phys. Plasmas* **8**, 2890–2907.

WOUCHUK, J.G. & NISHIHARA, K. 1997 Asymptotic growth in the linear Richtmyer–Meshkov instability. *Phys. Plasmas* **4**, 1028–1038.

YANG, Y., ZHANG, Q. & SHARP, D.H. 1994 Small amplitude theory of Richtmyer–Meshkov instability. *Phys. Fluids* **6**, 1856–1873.

ZHAI, Z., ZOU, L., WU, Q. & LUO, X. 2018 Review of experimental Richtmyer–Meshkov instability in shock tube: from simple to complex. *Proc. Inst. Mech. Engrs* C **232**, 2830–2849.

ZHANG, Q., DENG, S. & GUO, W. 2018 Quantitative theory for the growth rate and amplitude of the compressible Richtmyer–Meshkov instability at all density ratios. *Phys. Rev. Lett.* **121**, 174502.

ZHANG, Q. & GUO, W. 2016 Universality of finger growth in two-dimensional Rayleigh–Taylor and Richtmyer–Meshkov instabilities with all density ratios. *J. Fluid Mech.* **786**, 47–61.

ZHANG, Q. & SOHN, S. 1997 Nonlinear theory of unstable fluid mixing driven by shock wave. *Phys. Fluids* **9**, 1106–1124.

ZHOU, Y. 2017 Rayleigh–Taylor and Richtmyer–Meshkov instability induced flow, turbulence, and mixing. I. *Phys. Rep.* **720–722**, 1–136.

ZHOU, Y., CLARK, T.T., CLARK, D.S., GAIL GLENDINNING, S., AARON SKINNER, M., HUNTINGTON, C.M., HURRICANE, O.A., DIMITS, A.M. & REMINGTON, B.A. 2019 Turbulent mixing and transition criteria of flows induced by hydrodynamic instabilities. *Phys. Plasmas* **26**, 080901.